

Kramers-Kronig constrained variational analysis of optical spectra

A. B. Kuzmenko

*DPMC, University of Geneva, 24 Quai Ernest-Ansermet,
1211 Geneva 4, Switzerland*

A universal method of extraction of the complex dielectric function $\epsilon(\omega) = \epsilon_1(\omega) + i\epsilon_2(\omega)$ from experimentally accessible optical quantities is developed. The central idea is that $\epsilon_2(\omega)$ is parameterized independently at each node of a properly chosen anchor frequency mesh, while $\epsilon_1(\omega)$ is dynamically coupled to $\epsilon_2(\omega)$ by the Kramers-Kronig (KK) transformation. This approach can be regarded as a limiting case of the multi-oscillator fitting of spectra, when the number of oscillators is of the order of the number of experimental points. In the case of the normal-incidence reflectivity from a semi-infinite isotropic sample the new method gives essentially the same result as the conventional KK transformation of reflectivity. In contrast to the conventional approaches, the proposed technique is applicable, without readaptation, to virtually all types of linear-response optical measurements, or arbitrary combinations of measurements, such as reflectivity, transmission, ellipsometry *etc.*, done on different types of samples, including thin films and anisotropic crystals.

I. INTRODUCTION

The linear macroscopic optical characteristics of materials, such as reflectivity, absorption, penetration depth and others, are largely determined by the complex dielectric function $\epsilon(\omega) = \epsilon_1(\omega) + i\epsilon_2(\omega)$ ¹. Typically, one has to extract $\epsilon_1(\omega)$ and $\epsilon_2(\omega)$ of the studied sample by the inversion of measured optical spectra. These quantities are not independent, but comply the Kramers-Kronig (KK) relations^{2,3,4,5}:

$$\epsilon_1(\omega) - 1 = \frac{2}{\pi} \wp \int_0^\infty \frac{x\epsilon_2(x)}{x^2 - \omega^2} dx, \quad (1)$$

$$\epsilon_2(\omega) = -\frac{2\omega}{\pi} \wp \int_0^\infty \frac{\epsilon_1(x)}{x^2 - \omega^2} dx + \frac{4\pi\sigma_{DC}}{\omega}, \quad (2)$$

where σ_{DC} is the DC conductivity, and the symbol \wp denotes the principal value integral.

When talking about experimental ways to extract of ϵ_1 and ϵ_2 , one should distinguish between the ones that rely on the KK relations and the ones that allow the determination of both quantities directly from the experiment. A well-known example of the first type of techniques is the KK analysis of the normal-incidence reflectivity $R(\omega)$ spectra⁶. The idea of this method is the following. Equations (1) and (2) cannot be directly applied, since both ϵ_1 and ϵ_2 depend on the unknown phase θ of the complex reflectivity

$$r = \frac{1 - \sqrt{\epsilon}}{1 + \sqrt{\epsilon}} = \sqrt{R} \exp(i\theta). \quad (3)$$

A very helpful 'trick' is to write down a relation similar to (2) with respect to the complex function $\ln r(\omega) = \ln \sqrt{R(\omega)} + i\theta(\omega)$:

$$\theta(\omega) = -\frac{2\omega}{\pi} \wp \int_0^\infty \frac{\ln \sqrt{R(x)}}{x^2 - \omega^2} dx + \theta(0) \quad (4)$$

and use it to compute $\theta(\omega)$ from $R(\omega)$. The reflectivity has to be extrapolated outside the experimentally accessible frequency range, which may give rise to a large uncertainty, if the experimental range is not sufficiently broad⁷. Having found the reflectivity phase, one can restore the dielectric function by inverting (3): $\epsilon = (1 - r)^2 / (1 + r)^2$. Thus, the KK relation is an additional condition, which 'miraculously' helps to get two spectra, $\epsilon_1(\omega)$ and $\epsilon_2(\omega)$, out of one, $R(\omega)$.

Unfortunately, the approach based on equations like (4), is not universal⁸. The KK relations are derived for the so-called response functions⁴, which have regular analytical behavior in the upper complex frequency half-plane due to the causality principle. In the case of the function $\ln r(\omega)$, a necessary condition is that $r(\omega) \neq 0$ for $\text{Im}(\omega) > 0$. One can show, that it holds for the normal angle of incidence, but breaks down, for instance, for off-normal reflectivity, if the angle of incidence is large enough⁹. The same problem appears, when the sample is a thin film on a substrate and in many other cases. A number of analytical and numerical algorithms were put forward to extend the KK method to off-normal reflection^{9,10,11,12,13,14,15}, transmission^{16,17,18,19}, attenuated total reflection (ATR) spectra^{13,20,21,22} as well as to optical data on layered samples^{14,17,23,24,25,26,27} and low-symmetry crystals^{28,29} and other 'non-standard' situations. Although the proposed techniques, taken together, certainly cover a substantial scope of applications, it is desirable, from the practical point of view, to have a single universal approach, which can be used in most of the currently used and future optical experiments without major readaptation.

The least-square fitting of spectra using simple model dielectric functions, such as Drude-Lorentz oscillators, also called the dispersion analysis³⁰, is practically more robust^{26,31} than the mentioned above KK-based techniques. However, the range of considered dielectric functions is artificially restricted to a certain model, which makes it hard to recover, without distortions, all significant spectral details from the experimental data. On

the other hand, the introduction of new parameters to a model (for example, the addition of extra Lorentz oscillators), makes the functional form for the dielectric function more 'flexible' and, in a sense, less model-dependent.

The method of the *KK-constrained variational fitting*, developed in this paper, is a 'hybrid' of the two approaches. It inherits the robustness of the least-square fitting and the ability of the KK analysis to extract the full spectral information. In simple terms, it is a limiting case of the multi-oscillator modelling, when the number of oscillators is so large (of the order of the number of experimental points), that the analysis becomes essentially *model-independent*. Since the KK relations (1,2) are automatically preserved in the used functional form of the dielectric function, the proposed approach can also be regarded, as an extension of the standard KK methods.

The basic idea of the KK-constrained variational fitting was already introduced in Ref.²⁹ for the special case of the normal-incidence reflectivity of low-symmetry (monoclinic and triclinic) crystals, where the standard KK method fails. The KK relations for the diagonal and off-diagonal components of the reflectivity tensor were used, which limited the applicability of the technique. Here we overcome this limitation by referring directly to the KK relations for the dielectric function.

The rest of the manuscript is organized as follows. In Section II we outline the general problem targeted by the method. Section III discusses the variational fitting as a limiting case of the usual data fitting with a large number of oscillators. In Section IV we describe the technique in details. Section V contains a number of application examples. Finally, in Section VI we summarize the results and overview the possible future developments.

II. PROBLEM FORMULATION

We begin with a formal problem definition. Suppose, a set of experimental datapoints $\{\omega_i^{exp}, q_i^{exp}, \delta q_i^{exp}\}$ ($i=1, \dots, N_{exp}$) is given, where ω_i^{exp} is frequency, q_i^{exp} is an optical quantity of a certain type (reflectivity, transmission, penetration depth, an ellipsometric angle *etc.*) and δq_i^{exp} is an experimental error bar of q_i^{exp} . We assume, that all optical quantities can be expressed via real and imaginary parts of the material dielectric function $\epsilon(\omega)$:

$$q_i^{calc} = f_i(\epsilon_1(\omega_i^{exp}), \epsilon_2(\omega_i^{exp})). \quad (5)$$

Different datapoints can be of different types, therefore we keep the index i in f_i . Using the transformation (1) (which can be symbolically written as $\{\epsilon_1\} - 1 = KK(\{\epsilon_2\})$), we get:

$$q_i^{calc}(\{\epsilon_2\}) = f_i(1 + KK\{\epsilon_2\}(\omega_i^{exp}), \epsilon_2(\omega_i^{exp})). \quad (6)$$

Note that q_i^{calc} depends not only on ϵ_2 at ω_i^{exp} , but also on $\epsilon_2(\omega)$ at all other frequencies.

It is natural to look for a *dielectric function* $\epsilon(\omega)$, which satisfies the KK relations and provides the best fit of all

experimental datapoints:

$$\chi^2(\{\epsilon_2\}) \equiv \sum_{i=1}^{N_{exp}} \left(\frac{q_i^{calc}(\{\epsilon_2\}) - q_i^{exp}}{\delta q_i^{exp}} \right)^2 \rightarrow \min. \quad (7)$$

This relation formalizes the least-square approach, which is justified in the case of the normal error distribution³².

The minimization problem (7) is not fully defined unless we specify the functional space for $\epsilon_2(\omega)$. In principle, one may consider all physically acceptable functions $\epsilon_2(\omega)$ ($0 \leq \omega < \infty$), which are non-negative and integrable (*i.e.* compatible with the f-sum rule^{4,5}):

$$\int_0^\infty x \epsilon_2(x) dx < \infty. \quad (8)$$

However, in such a broad functional space the minimization problem becomes *ill-posed*³³. In particular, multiple solutions for $\epsilon_2(\omega)$ may exist, which look very different, but minimize (7) equally well. However, if the set of datapoints is sufficiently broad and dense, only one (or maybe few) solutions will show a regular behavior, while the majority of them will be marked by 'suspicious' features, for instance, sharp spikes, discontinuities or oscillations with a period smaller than the distance between experimental frequencies.

It suggests that a proper way to regularize this ill-posed problem is to restrict somehow the functional space $\epsilon_2(\omega)$. It can be done using some parametrization, for example, the decomposition of $\epsilon_2(\omega)$ in a finite basis of fixed reference functions. An optimal parametrization should exclude the mentioned irregular features, while being flexible enough to fit all important spectral details. Without rigorous mathematical proof, but rather based on practical tests, we argue that *the optimal number of parameters should be of the order of, but not larger than, N_{exp}* .

One should note that it is more common to use model dielectric functions with a small number of parameters, much less than N_{exp} . In this case, the purpose of the analysis is to get a *physical insight* using the measured spectra directly. For instance, the validity of a certain hypothesis about the studied compound can be tested and the values of some meaningful parameters (such as the plasma frequency, optical transition energies *etc.*) can be found. On the contrary, the purpose of parametrization in the *model-independent* method, proposed in this paper, is not to get the values of parameters (which may have almost no physical meaning, taken alone), but rather to extract the complex dielectric function by the inversion of the available data. Thus, it is not surprising that the number of parameters becomes very large. The minimization of (7) in this case is essentially a *variational* problem. The obtained in this way dielectric function can be used later on for a more specific examination.

III. DRUDE-LORENTZ FITTING AS A PARAMETRIZATION

An important example of parametrization of dielectric functions is the Drude-Lorentz (DL) oscillators formula

$$\epsilon(\omega) = \epsilon_\infty + \sum_{k=1}^N \frac{\omega_{p,k}^2}{\omega_{0,k}^2 - \omega^2 - i\omega\gamma_k}. \quad (9)$$

Each oscillator is represented by a Lorentzian with three adjustable parameters: the oscillator frequency ω_{0k} , the linewidth γ_k and the plasma frequency $\omega_{p,k}$. The unbound oscillators (conductivity electrons) are described by Drude terms, where $\omega_{0,k} = 0$. The parameter ϵ_∞ is the contribution from the higher-frequency oscillators.

Usually the number of oscillators is very limited, compared to N_{exp} . As a result, the obtained spectra of $\epsilon(\omega)$ are 'unrealistically' smooth with some subtle, but potentially important, spectral information being lost. According to previous arguments, one should take a very large number of oscillators (of the order of N_{exp}) in order to extract the information model-independently. It was argued (see Refs.^{26,31}) that the fitting of the most important details of spectra (other than statistical noise) is not much different from the KK transformation. The physical meaning of individual oscillator terms may not be always clear, however, the meaningful result is the complex value of $\epsilon(\omega)$ itself.

In practice, the oscillators are usually introduced one by one and all Lorentzian parameters are allowed to change. Although this strategy works very well for small N ($\sim 10 - 20$), it becomes cumbersome and badly controlled as the number of oscillators grows further. In particular, as one adds more and more Lorentzians to the model function (9), it becomes less and less clear how to guess the initial parameter values. If all parameters are free to change, it often happens that the fitting process becomes numerically unstable. To avoid it, one has to deliberately fix some parameters. It makes the fitting procedure rather tricky and ambiguous, preventing the routine operation. In the next section we elaborate another fitting scheme which is more attractive from the practical point of view.

IV. METHOD

Now we proceed with the detailed description of the KK-constrained variational fitting algorithm. Although it can be concisely described in a hand-book like manner, we prefer to show its 'evolution' starting from the described above DL fitting scheme. In this way, one can easily see that the new technique is, in principle, a limiting case of the multi-oscillator fitting.

A. Setting up the oscillators

Let us consider a dense enough mesh of anchor frequency points $\omega_1, \dots, \omega_N$. It must not be the same as the set of experimental frequencies $\omega_1^{exp}, \dots, \omega_{N_{exp}}^{exp}$, introduced in Section II, although they may coincide. We shall discuss below the optimal choice of the anchor mesh.

It is possible to set the number of oscillators in (9), their frequencies and linewidths in a rather logical and simple way. To be 'flexible enough', the fitting function (9) should be able to deliver spectral weight *everywhere* in the spectral range. It can be done by putting one separate oscillator *at every anchor frequency*: $\omega_{0,i} = \omega_i$. Furthermore, we would like the i -th oscillator to be narrow and provide spectral weight only in the closest neighborhood of ω_i . It suggests to set its width to a fixed value of the order of the distance between adjacent frequency points, for instance $\gamma_i = (\omega_{i+1} - \omega_{i-1})/2$. Figure 1(a) shows the real and the imaginary part of the i -th Lorentzian:

$$\epsilon_{1,i}^{Lor}(\omega) = \frac{\omega_{p,i}^2(\omega_i^2 - \omega^2)}{(\omega_i^2 - \omega^2)^2 + \gamma_i^2\omega^2} \quad (10)$$

$$\epsilon_{2,i}^{Lor}(\omega) = \frac{\omega_{p,i}^2\omega\gamma_i}{(\omega_i^2 - \omega^2)^2 + \gamma_i^2\omega^2} \quad (11)$$

In this way we get a dense 'forest' of narrow Lorentzians, sitting at fixed anchor frequencies. Only the oscillator strengths S_i are left adjustable in order to set up the profile of the 'forest'.

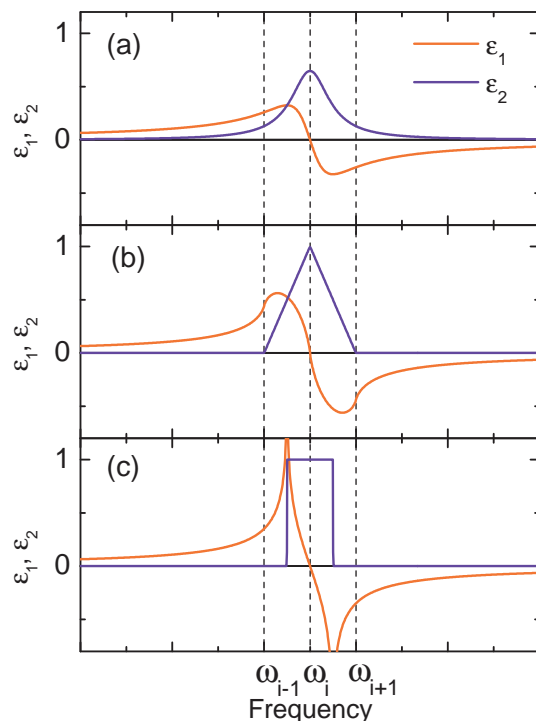


FIG. 1: Dielectric functions with a Lorentz (a), a triangular (b) and a rectangular (c) lineshapes, centered at ω_i and having the linewidth $\gamma_i = (\omega_{i+1} - \omega_{i-1})/2$.

B. Optimizing the oscillator lineshape

Because of extended low- and high-frequency tails, which interfere with other oscillators, the Lorentz lineshape (Figure 1(a)) is not very suitable to represent the 'local' spectral weight near ω_i ³⁴. The problem becomes evident from the following example. Imagine, that there is a low-frequency gap ω_g in the spectrum: $\epsilon_2(\omega) = 0$ for $\omega < \omega_g$. However, each Lorentzian that we have to put above ω_g is going to contribute a non-zero value of ϵ_2 below ω_g because of its low-frequency tail. This makes a good fitting quality with Lorentzian oscillators hardly achievable.

Clearly, it is better to have a lineshape function, which is non-zero only inside a small region, adjacent to ω_i . A good candidate is a triangular profile, shown on Figure 1(b):

$$\epsilon_{2,i}^{\Delta}(\omega) = \begin{cases} (\omega - \omega_{i-1})/(\omega_i - \omega_{i-1}) & , \omega_{i-1} < \omega \leq \omega_i \\ (\omega_{i+1} - \omega)/(\omega_{i+1} - \omega_i) & , \omega_i < \omega < \omega_{i+1} \\ 0 & , \text{otherwise} \end{cases} \quad (12)$$

The real part can be obtained by the KK transformation (1):

$$\epsilon_{1,i}^{\Delta}(\omega) = \frac{1}{\pi} \left[\frac{g(\omega, \omega_{i-1})}{\omega_i - \omega_{i-1}} - \frac{(\omega_{i+1} - \omega_{i-1})g(\omega, \omega_i)}{(\omega_i - \omega_{i-1})(\omega_{i+1} - \omega_i)} + \frac{g(\omega, \omega_{i+1})}{\omega_{i+1} - \omega_i} \right] \quad (13)$$

with $g(x, y) \equiv (x + y) \ln |x + y| + (x - y) \ln |x - y|$.

Exactly as we did it before, the variational dielectric function can be constructed as a linear superposition of triangular functions sitting at fixed anchor frequencies ω_i :

$$\epsilon_{var}(\omega) = \sum_{i=2}^{N-1} A_i \epsilon_i^{\Delta}(\omega) \quad (14)$$

The coefficients A_i are tread as *free* parameters. We excluded $i = 1$ and $i = N$, from the summation by defining $A_1 = A_N = 0$.

The variational function is shown schematically on Figure 2. The imaginary part of $\epsilon_{var}(\omega)$ is a piecewise curve passing through points $\{\omega_i, A_i\}$ ($i = 1 \dots N$). Thus, the adjustable parameters have very straightforward meaning: they are the values of ϵ_2 at anchor frequencies ω_i . Obviously, any shape of $\epsilon_2(\omega)$ of a real material can be reproduced with a proper set of parameters A_i , provided that the frequency mesh is dense enough.

At first glance, a triangular lineshape is rather 'pathological' for an oscillator. However, we are going to ascribe the physical meaning not to the individual oscillators, but to the total dielectric function (14), composed of many of them. It makes us free to choose a lineshape, which is the most convenient from the computational point of view. Even though this choice is rather arbitrary, it is not crucial for the method. It is equivalent to a decision

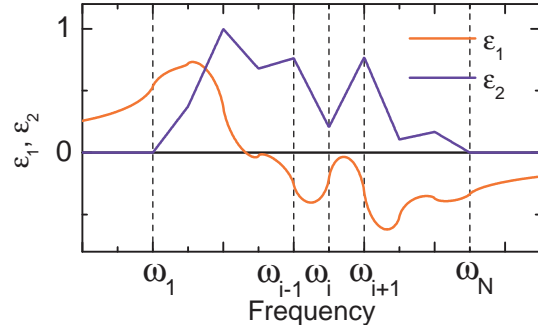


FIG. 2: An example of the variational dielectric function $\epsilon_{var}(\omega)$, described in the text. The imaginary part of ϵ_{var} is a superposition of several triangular functions $\epsilon_{2,i}^{\Delta}(\omega)$, centered at anchor frequencies. $\epsilon_{1,var}(\omega)$ is the exact KK transform of $\epsilon_{2,var}(\omega)$.

of which quadrature formula to use for the numerical integration in the KK transformation. The triangular lineshape shape corresponds to the trapezoidal integration. One can also use a rectangular shape of $\epsilon_{2,i}^{\Delta}(\omega)$ (Figure 1(c)). However, it is inferior to $\epsilon_{2,i}^{\Delta}(\omega)$, since the discontinuity of $\epsilon_{2,i}^{\Delta}(\omega)$ would result in artificial divergences of $\epsilon_{1,i}^{\Delta}(\omega)$ at the rectangle edges.

C. Discrete Kramers-Kronig transform

Since we deal with the values of the dielectric function at a fixed mesh, it is convenient to represent its real and imaginary parts as vectors: $\epsilon_{1,i} \equiv \epsilon_1(\omega_i)$ and $\epsilon_{2,i} \equiv \epsilon_2(\omega_i)$. Then, using formulas (14) and (13), the KK transform (1) can be represented in a matrix form:

$$\epsilon_{1,i} - 1 = \sum_{j=1}^N K_{ij} \epsilon_{2,j}, \quad (15)$$

where

$$K_{ij} = \epsilon_{1,j}^{\Delta}(\omega_i). \quad (16)$$

Keeping in mind the analogy with the discrete Fourier transform, we can call (15) a *discrete Kramers-Kronig transform* (DKKT). The matrix K_{ij} is a discrete analog of the KK kernel $K(x, \omega) \equiv (2/\pi)x(x^2 - \omega^2)^{-1}$ in (1). The exact expression for the DKKT depends, of course, on the chosen oscillator lineshape. However, for $|i-j| \geq 2$ all lineshapes give almost the same value of K_{ij} .

D. The problem of extrapolations

A serious shortcoming of the variational function (14), taken alone, is that it does not take into account any spectral weight beyond the frequency range $\omega_1 < \omega < \omega_N$. Due to the non-local character of the KK relation (1),

the non-zero wings of ϵ_2 at higher and lower frequencies are essential to calculate ϵ_1 inside this region. Therefore, some assumptions about the high- and low-frequency behavior of ϵ_2 should be taken.

The same problem of extrapolations exists in the usual KK analysis of reflectivity, which does not have any universal solution. Nevertheless, an 'educated guess' can often be done, based on some reasonable physical model. We argue that the following 'two-step' fitting scheme can address the issue of the extrapolations.

At first, the experimental spectra can be fitted in a conventional way by some formula-defined dielectric function $\epsilon_{mod}(\omega)$ with a limited number of parameters. It can be a DL function (9) or a more appropriate physical model. If $\epsilon_{mod}(\omega)$ describes the major features of experimental spectra then we can assume that it gives an approximately correct frequency dependence outside the considered spectral range, even though some fine spectral details may not be fitted very well. Of course, in order to have a better confidence in the extrapolations, the experimental spectral range has to be expanded as much as possible, which is also true for the conventional KK analysis of reflectivity.

The next step is to add the variational function (14):

$$\epsilon_{total}(\omega) = \epsilon_{mod}(\omega) + \epsilon_{var}(\omega), \quad (17)$$

to 'fix' the parameters of $\epsilon_{mod}(\omega)$, and to perform the final data fitting with only parameters A_i of the variational function (14) kept adjustable. The low- and the high-frequency spectral weights are now accounted for by $\epsilon_{mod}(\omega)$. In this case the 'flexible' function $\epsilon_{var}(\omega)$ acts as a *small correction*, intended to fit the fine spectra details, unaccessible for the 'stiff' $\epsilon_{mod}(\omega)$. Therefore, the initial guess values A_i can be set to zero. Note that even though $\epsilon_{2,total}(\omega)$ ought to be positive, the sign of $\epsilon_{2,var}(\omega)$ is now arbitrary.

E. Computational details

Once the set of datapoints, the physical models and the anchor mesh are specified, one can minimize the chi-square functional (7) using of the standard non-linear minimization algorithms. In particular, the Levenberg-Marquardt (LM) method³² has proven to be very efficient, when the number of parameters is large. An important advantage of the LM algorithm is that it involves the calculation of derivatives of the model spectra with respect to parameters using explicit analytical formulas.

The optimization of the mesh of anchor frequencies $\omega_1, \dots, \omega_N$ is rather important for the correct work of the variational fitting routine. On one hand, the mesh should be dense enough to enable the variational function (14) to fit all important spectral details. On another hand, N should not be too large. The first reason is that the calculation time grows quickly as a function of the number of parameters to be adjusted. The second reason, discussed in Section II, is that an excessive 'flexibility' may

cause irregular behavior of the resulting functions, such as fast spurious oscillations. According to our experience, for an optimal mesh, N is two times smaller, than N_{exp} , while every anchor point corresponds to at least one experimental point, contributing to formula (7). On an everyday-use computer, one can handle up to few thousands parameters within reasonable time bounds, which is sufficient in most cases.

Another way to avoid physically meaningless numerical oscillations would be to add extra 'regularization' terms to the total chi-square functional (7), intended to make unfavorable those solutions, which have short-period oscillations. In this paper we are not going to discuss the details of possible regularization schemes. This work is in progress.

If the mesh optimization and other precautions fail to get rid of a numerical instability, it may signal that the systematic error bars are too large, or an inappropriate physical model is used. Such 'inconsistency alert', which is missing in the usual KK method, is another advantage of the proposed technique.

V. APPLICATION EXAMPLES

Now we turn to examples, showing the applications of the method. All calculations were performed using Reffit software³⁵, designed for the fitting of optical spectra with various physical models as well as the KK-constrained variational dielectric functions. As an experimental input, we shall use either really measured curves, or computer-generated test spectra.

A. Normal-incidence reflectivity

Let us first apply the variational fitting method to a normal-incidence reflectivity spectrum and compare it with the results of the usual KK analysis⁶. Figure 3(a) shows the far-infrared room-temperature reflectivity of a high- T_c superconductor $\text{Bi}_2(\text{Sr}, \text{Y})_2\text{CaCu}_2\text{O}_8$ (shortly Bi-2212) for the electric field along the c-axis (perpendicular to the planes CuO_2). The spectrum is dominated by optical phonons, since the interplane electronic transport is almost blocked.

We applied the usual KK analysis, extrapolating the reflectivity by a constant value at high and low frequencies, because the conductivity of Bi2212 along the c-axis is very small.

In order to perform the variational fitting, we took a mesh of 700 anchor frequencies, logarithmically distributed between $\omega_1 = 60 \text{ cm}^{-1}$ and $\omega_N = 1500 \text{ cm}^{-1}$. The resulting real and imaginary parts of $\epsilon(\omega)$ are shown in Figure 3(b) and (c). One can see that the two techniques give almost identical results in this reference case, when the conventional KK transform of reflectivity is known to be operational.

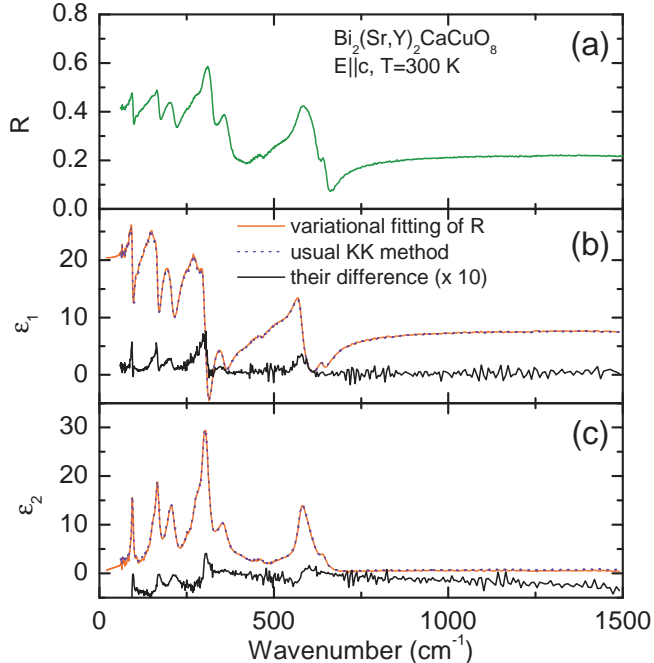


FIG. 3: The KK-constrained variational fitting vs. the usual KK analysis, applied to the normal-incidence reflectivity of Bi-2212 for $\mathbf{E} \parallel \mathbf{c}$, at room temperature (a). The two methods give almost indistinguishable $\epsilon_1(\omega)$ (b) and $\epsilon_2(\omega)$ (c). The difference between the results, multiplied by 10, is shown for comparison.

B. Grazing-incidence reflectivity

The measuring of reflectivity $R_p(\omega)$ at a grazing angle of incidence (close to 90°) for the polarization of light in the plane of incidence (p-polarization) is often preferable for highly reflecting metallic samples, since the measured absorption $A = 1 - R_p$ is more sensitive to the sample conductivity³⁶, than it is for the normal reflectivity. We are going to show that the variational fitting method is workable in the case of the off-normal incidence reflectivity. Here we use an artificial example, where the 'true' dielectric function is known beforehand.

The 'true' dielectric function $\epsilon(\omega) = \epsilon_1(\omega) + 4\pi i\sigma_1(\omega)/\omega$, which is shown in Figure 4 (b) and (c), was simulated by a DL model (9) with 10 randomly put Lorentz oscillators, one Drude peak and $\epsilon_\infty=6$. The 'experimental' reflectivity for the p-polarized light for the angle of incidence $\theta=80^\circ$ was calculated by the Fresnel formula⁵:

$$R_p = \left| \frac{\epsilon \cos \theta - \sqrt{\epsilon - \sin^2 \theta}}{\epsilon \cos \theta + \sqrt{\epsilon - \sin^2 \theta}} \right|^2.$$

Some statistical noise of 1% was added (red solid line on Figure 4 (a)) in order to mimic a real-life situation. We verified that the usual KK analysis does not work in this case: the formula (4), when applied to R_p , gives a totally wrong reflectivity phase spectrum.

The obtained in this way $R_p(\omega)$ was taken as an input for the KK-constrained variational fitting procedure. At the first stage the rough fitting was performed with only 3 oscillators included to $\epsilon_{mod}(\omega)$ (green dashed line on Figure 4 (a)). After that a variational function $\epsilon_{var}(\omega)$ was added to $\epsilon_{mod}(\omega)$ and the fine fitting of $R_p(\omega)$ was done. We took a mesh of 500 anchor frequency points, logarithmically distributed between 50 cm^{-1} and 10000 cm^{-1} . The resulting $\epsilon_1(\omega)$ and $\sigma_1(\omega)$ (Figures 4 (b) and (c), red line) are very close (apart from the noise) to the 'true' ones (Figure 4 (b) and (c), blue line). Of course, such a good agreement is only possible, when the frequency range of the input reflectivity spectrum is large enough.

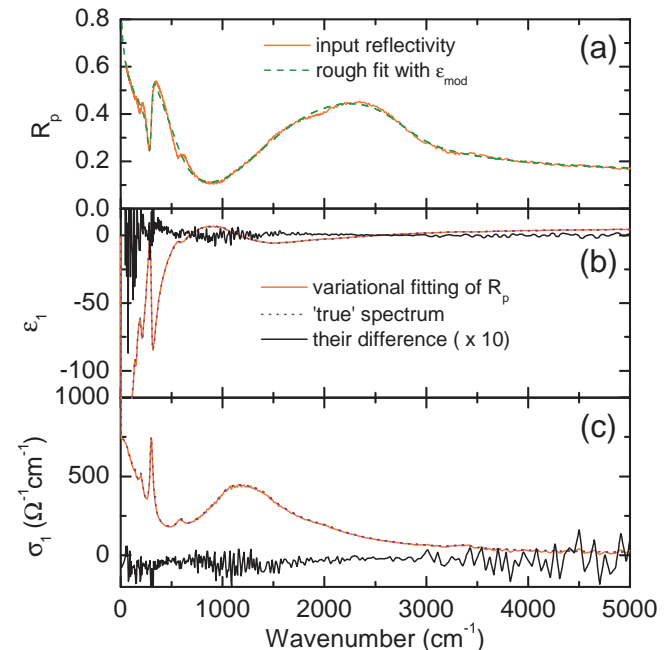


FIG. 4: The KK-constrained variational fitting of a grazing-incidence reflectivity spectrum for $\theta=80^\circ$ (a, red solid curve), simulated, using 10 Lorentz and 1 Drude oscillators as described in the text. The rough 3-oscillator fit is shown by the dashed green curve. The resulting $\epsilon_1(\omega)$ (b) and $\sigma_1(\omega)$ (c) are very close to the 'true' spectra. The difference between the results, multiplied by 10, is shown for comparison.

An example of the application of this procedure to a really measured grazing-incidence reflectivity spectrum (in combination with ellipsometry at higher frequencies) can be found in Ref.³⁷.

C. Reflectivity + transmission

Now we consider an example, when two measured spectra of *different types* are analyzed simultaneously. Figure 5(a) shows reflectivity and transmission spectra of $\text{La}_{1.88}\text{Sr}_{0.12}\text{CuO}_4$ (LSCO) in the far- and mid-infrared range at room temperature³⁸. The electric field was al-

ways parallel to the c -axis. The near-normal incidence reflectivity $R(\omega)$ was measured on a thick non-transparent sample. The transmission spectrum $T(\omega)$ was taken on a thin slab of the same material with a thickness $d=23 \mu\text{m}$. Both spectra can be expressed in terms of the complex dielectric function $\epsilon(\omega)$ ⁵:

$$R = |r|^2, T = \left| \frac{(1-r^2)t}{1-r^2t^2} \right|^2, \quad (18)$$

where

$$r = \frac{1 - \sqrt{\epsilon}}{1 + \sqrt{\epsilon}}, t = \exp\left(i\frac{\omega}{c}\sqrt{\epsilon}d\right).$$

The formula for T takes into account multiple internal reflections, which give rise to Fabry-Perot interference fringes. Unfortunately, the fringes are partially suppressed in the experiment, because the sample was not exactly flat-parallel. This was taken into account by the averaging of T for a certain distribution (about 10%) of the sample thicknesses.

Figure 5(b) shows the optical conductivity $\sigma_1(\omega)$, obtained by two different techniques: the standard KK transformation of reflectivity (not considering the transmission spectrum) and the KK constrained variational simultaneous fitting of reflectivity and transmission (which we call RT+KK method³⁸). The c -axis conductivity is featured by a slowly varying small electronic conductivity, determined by an incoherent electron transport along the c -axis, and the two strong phonon peaks at 235 and 495 cm^{-1} .

One can notice, that the two techniques give similar results in the phonon range, but significantly deviate at lower and especially at higher frequencies (watch the log scale!), where the conductivity is small. It is not surprising, since the reflectivity in this case depends mostly on the ϵ_1 and is not very sensitive to σ_1 . Thus, the error bars of the latter are very large. On the other hand, the transmission is directly related to the absorption, and, correspondingly, to the conductivity. Therefore, it is really worthwhile to use both $R(\omega)$ and $T(\omega)$ in the analysis.

The advantage of using the KK constraint here is not immediately obvious, since the two values R and T can be in principle converted to ϵ_1 and σ_1 at every given frequency (RT-method). However, this conversion works well only if the value of transmission is not too small. In our case the transmission vanishes between 200 and 600 cm^{-1} (in the phonon range), where we have to resort to the KK relations. Using two different techniques in different ranges would not be very practical. Alternatively, the RT+KK method provides a seamless conductivity spectrum with small error bars in the whole spectral range. In addition, the using of the transmission spectrum outside the phonon range in the RT+KK technique suppresses the uncertainties of the KK analysis due to the high- and low-frequency extrapolations. A similar idea of 'phase anchoring' is discussed in the next example.

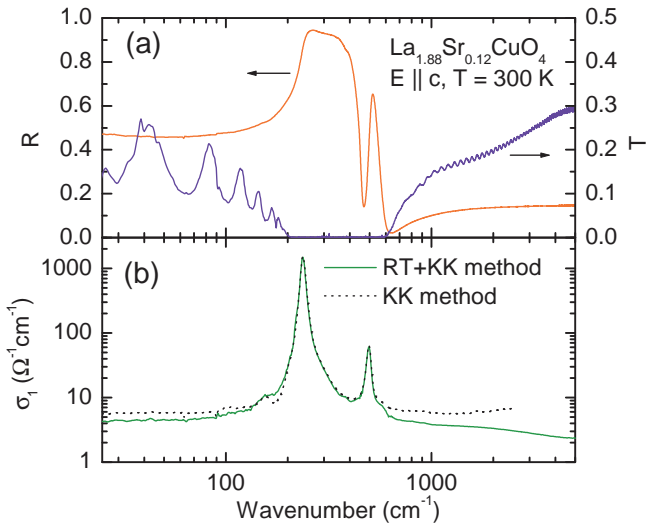


FIG. 5: Reflectivity (bulk sample) and transmission (thin 23 μm sample) of LSCO for $E||c$ at room temperature. (b) The conductivity spectrum obtained by the RT+KK analysis, as described in the text.

D. Low-frequency reflectivity + high-frequency ϵ_1 and ϵ_2

It is known, that the accuracy of the KK analysis can be greatly improved if both real and imaginary parts of $\epsilon(\omega)$ are measured *independently* in selected frequency points^{39,40} or in a certain interval^{41,42}. Here we consider a situation, when one can obtain $\epsilon_1(\omega)$ and $\epsilon_2(\omega)$ at high frequencies, but only the reflectivity $R(\omega)$ can be measured at low frequencies.

In order to extract the conductivity at low frequencies, we have to use the KK relations. It is desirable to take as much profit as possible from the knowledge of both ϵ_1 and ϵ_2 at high frequencies. Therefore, it would be rather wasteful, for example, to calculate R from ϵ_1 and ϵ_2 at high frequencies and use it only to extend the range for the usual KK transformation (4). On the other hand, the simultaneous KK-constrained fitting of the low-frequency reflectivity and the high-frequency $\epsilon_1(\omega)$ and $\epsilon_2(\omega)$ ^{31,37,43} allows one to use all available information, in particular, to 'anchor' the phase of the reflectivity.

An example is shown on Figure 6. The data were taken on a polycrystalline sample of MgB_2 , which is a good metal. Even though the magnesium diboride is an anisotropic compound, in the spectra analysis it was assumed that the powder sample behaves as an optically isotropic one, described by an effective dielectric function $\epsilon(\omega)$. The reflectivity at a nearly normal incidence was measured in the range 20 - 6000 cm^{-1} (Figure 6(a)), and the ellipsometry at an angle of incidence $\theta=80^\circ$ provided $\epsilon_1(\omega)$ and $\epsilon_2(\omega)$ at 6000-37000 cm^{-1} (Figure 6(b)).

The variational fitting was done in the same way, as described before. The anchor mesh covered both spectral ranges. The quality of the variational fit is very good, giving confidence in the resulting optical conduc-

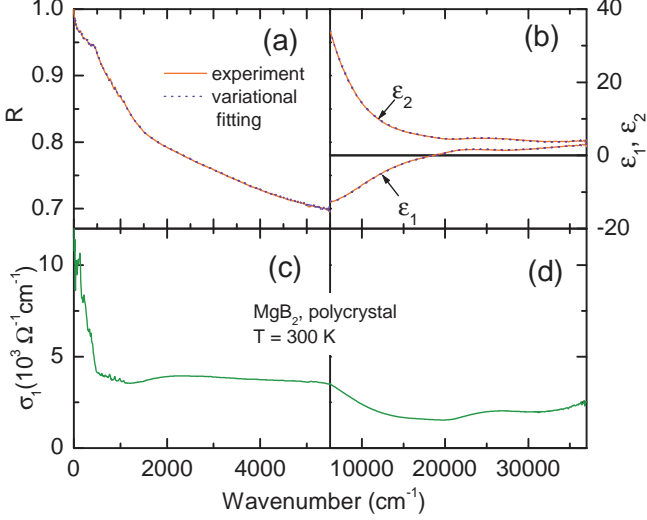


FIG. 6: The KK-constrained variational fitting of the reflectivity in the far- and mid-IR (a) and $\epsilon_1(\omega)$ and $\epsilon_2(\omega)$ in the near-infrared to UV ranges of a polycrystalline sample of MgB_2 at room temperature. The panels (c) and (d) show the obtained effective optical conductivity.

tivity spectrum (Figure 6(c-d)).

E. Reflectivity of a thin film on a substrate

The next example shows that the method can also be used to analyze optical data of layered samples. We shall consider a simple but practically very important case of an optically thin film grown on a substrate. If the penetration depth is comparable, or larger than the film thickness then the substrate contributes to the overall optical response. One has to take it into account, when extracting optical properties of the film from the reflectivity spectra²⁶.

We generate dielectric functions of the film $\epsilon_f(\omega)$ and the substrate $\epsilon_s(\omega)$ in the infrared range using certain models in order to check later on the accuracy of the final result. For the substrate we took a model that gives optical properties close to the ones of SrTiO_3 ⁴⁴, often used as a substrate material. The reflectivity $R(\omega)$ and optical conductivity $\sigma_1(\omega)$ of the substrate are shown by green curves in Fig. 7 (a) and (b) respectively. The infrared spectrum of SrTiO_3 is dominated by strong phonon lines at 100, 180 and 550 cm^{-1} . To simulate the properties of the film, a model was taken, which gives a metallic conductivity with a plasma edge at around 10000 cm^{-1} and some additional double-peak structure at about 300 - 400 cm^{-1} . The corresponding $R(\omega)$ (for a bulk sample) and $\sigma_1(\omega)$ are presented in Fig. 7 (blue curves).

The normal-incidence 'experimental' reflectivity of the film+substrate system was calculated using formula⁵

$$R = \left| \frac{r_f + t^2 r_{fs}}{1 + t^2 r_f r_{fs}} \right|^2, \quad (19)$$

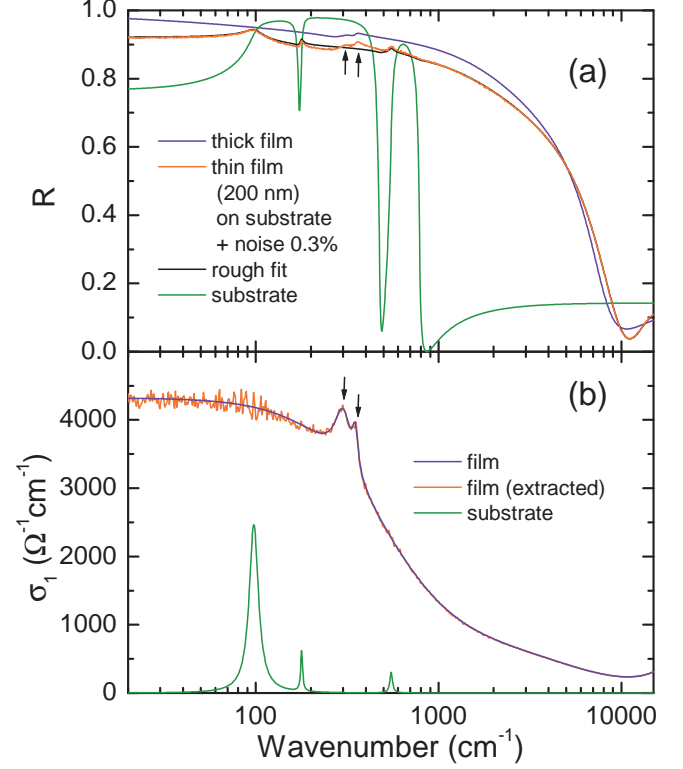


FIG. 7: A test example of the KK-constrained variational fitting of a reflectivity spectrum measured on a thin film (200 nm) grown on a substrate with known optical properties. The test dielectric functions of the film and the substrate were generated as described in the text. The panel (a) shows the generated reflectivity of a thick film (blue), the one of the thin film (red), used as an input, with a noise of 0.3% added, and the one of a bare substrate (green). The black curve is the initial rough fit of the 'measured' reflectivity. The panel (b) indicates the exact optical conductivity of the film (blue), the extracted one by the method (red) and the conductivity of the substrate itself (green). On both panels the arrows mark the optical peaks, which come from the film.

where

$$r_f = \frac{1 - \sqrt{\epsilon_f}}{1 + \sqrt{\epsilon_f}}, r_{fs} = \frac{\sqrt{\epsilon_f} - \sqrt{\epsilon_s}}{\sqrt{\epsilon_f} + \sqrt{\epsilon_s}}, t = \exp\left(i\frac{\omega}{c}\sqrt{\epsilon_f}d\right)$$

for the film thickness d of 200 nm (the red curve in Fig.7(a)). Some artificial noise of 0.3% was added, in order to check the influence of the statistical errors on the result. One can see that the reflectivity spectrum of the thin films is very different from the one of a thick sample. The structures in the far-infrared range are caused not only by peaks in the film conductivity (shown by arrows), but also by the phonon lines of the substrate.

As usual, the fitting process was done in two steps. Initially, the 'experimental' spectrum was fitted with a very limited model $\epsilon_{mod}(\omega)$. The corresponding reflectivity is shown by the black curve in Fig.7(a). Secondly, the variational fitting was performed, using ϵ_{var} , defined on about 500 anchor frequency nodes (one-half of the total

number of experimental points).

The resulting optical conductivity is shown by the red curve in Fig.7(b). The agreement with the exact conductivity is rather good. The double-peak structure, which was not described by the initial limited model, is reproduced quite well. One can see that the experimental noise has little effect at high frequencies, but is strongly amplified below 200 cm^{-1} . This is hardly surprising, since the KK method is known to produce large error bars for metallic samples at low frequencies, where the reflectivity is close to 1.

VI. SUMMARY

We introduced a new technique of the extraction of the real and the imaginary parts of the dielectric function from optical spectra. The idea is that all available data-points are fitted simultaneously, using a dielectric function, which has a fully flexible (variational) imaginary part $\epsilon_2(\omega)$ and the real part $\epsilon_1(\omega)$, dynamically coupled to the $\epsilon_2(\omega)$ via the KK relation. In simple cases the method works as well, as the usual KK transformation of reflectivity.

It was shown that the scope of applications of the variational KK-constrained fitting is extremely broad. It extends to various optical techniques, or combinations of them, as well as to different types of samples. The computational time required for a typical KK-constrained fitting session is somewhat longer, compared to the usual KK transformation, but it is yet well within reasonable limits. It is important, that the method needs almost no readaptation for different experimental situations, saving a lot of human time.

Certain optical methods, such as spectroscopic ellipsometry, or a combination of reflection and transmission do not formally rely the KK relations, since both ϵ_1 and

ϵ_2 can be obtained directly from the measured data at each frequency. Even though the independence on the KK relation is a big advantage of such techniques, the method, proposed in this paper, can yet be very useful here as a stringent test on the overall KK consistency of the experimental data.

In this article we assumed that the materials under study are non-magnetic, which means that magnetic permeability μ is equal to 1. For magnetic materials, the method can be used to determine $\mu(\omega)$, which also satisfies the KK relations. Of course, in order to disentangle $\mu(\omega)$ and $\epsilon(\omega)$ one may need to analyze several measurements simultaneously (for instance, the transmission of samples of different thicknesses).

So far we discussed the linear-response optical measurements only, but, of course, the range of subjects, where the KK relations are used, is not restricted to the linear optics. The method is potentially applicable to any spectroscopic technique, where the measured spectra depend on a combination of real and imaginary parts of a causal, a therefore KK-compliant, response function to be determined. The examples include photoemission, neutron scattering⁴⁵, X-ray spectroscopy^{2,3,46}, electron energy loss spectroscopy (EELS)⁴⁷, magneto optical Kerr effect (MOKE)⁴⁸, Josephson-contact spectroscopy^{49,50}, electrode impedance measurements⁵¹, electron spin resonance (ESR)^{52,53}, low-energy electron diffraction (LEED)⁵⁴, acoustics^{55,56} and others. Since KK-type relations exist for higher-order susceptibilities^{57,58}, this way to analyze data can also be useful in non-linear spectroscopic techniques.

The author is grateful to D. van der Marel, F. P. Mena, H. J. A. Molegraaf and F. Carbone for numerous discussions and invaluable practical help. Useful advices about solutions of ill-posed inverse problems were given by S. V. Rotin.

¹ Here we assume that the magnetic permeability $\mu = 1$ and the effects of the spatial dispersion are negligible, or, in other words, $\epsilon(\omega)$ can be regarded as momentum-independent.

² H. A. Kramers, *Nature* **117**, 775 (1926).

³ R. de Kronig, *J. Opt. Soc. Am.* **12**, 547 (1926).

⁴ L. D. Landau and E. M. Lifshitz, *Electrodynamics of Continuous Media*, Oxford, Pergamon Press (1975).

⁵ M. Dressel and G. Grüner, *Electrodynamics of Solids*, Cambridge University Press (2002).

⁶ F. C. Jahoda, *Phys. Rev.* **107**, 1261 (1957).

⁷ D. E. Aspnes, *The Accurate Determination of Optical Properties by Ellipsometry*, in *Handbook of Optical Constants of Solids* ed. by E. D. Palik, Academic Press, Boston (1985).

⁸ W. G. Chambers, *Infrared Phys.* **15**, 139 (1975).

⁹ H. S. Somal, PhD thesis, University of Groningen (1998).

¹⁰ G. M. Hale, W. E. Holland, and M. R. Querry, *Appl. Opt.* **12**, 48 (1973).

¹¹ E. G. Makarova and V. N. Morozov, *Opt. Spectrosc.* **40**, 138 (1976).

¹² L. I. Alperovich and V. N. Pushkarev, *Opt. Spectrosc.* **47**, 516 (1979).

¹³ J. A. Bardwell and M. J. Dignam, *J. Chem. Phys.* **83**, 5468 (1985).

¹⁴ P. Grosse and V. Offermann, *Appl. Phys. A, Solids Surf.* **A52**, 138 (1991).

¹⁵ V. Hopfe, P. Bussemer, E. Richter, and P. Klobes, *J. Phys. D, Appl. Phys.* **25**, 288 (1992).

¹⁶ J. D. Neufeld and G. Andermann, *J. Opt. Soc. Am.* **62**, 1156 (1972).

¹⁷ R. D. Bringans, *J. Phys. D, Appl. Phys.* **10**, 1855 (1977).

¹⁸ K. Yamamoto and H. Ishida, *Vib. Spectrosc.* **15**, 27 (1997).

¹⁹ C.-P. E. Varsamis, *Appl. Spectrosc.* **56** 1107-13 (2002).

²⁰ A. E. Tshmel and V. I. Vettegren, *Spectrochim. Acta A, Mol. Spectrosc.* **29A**, 1681 (1973).

²¹ K. Yamamoto, A. Masui, and H. Ishida, *Appl. Opt.* **33**, 6285 (1994).

- ²² J. E. Bertie and Lan Zhida, *J. Chem. Phys.* **105**, 8502 (1996).
- ²³ E. A. Lupashko, V. K. Miloslavskii, and I. N. Shklyarevskii, *Opt. Spectrosc.* **29**, 419 (1970).
- ²⁴ W. J. Plieth and K. Naegle, *Surf. Sci.* **50**, 53 (1975).
- ²⁵ A. V. Tikhonravov and I. V. Zuev, *Mosc. Univ. Phys. Bull.* **48**, 44 (1993).
- ²⁶ A. F. Santander-Syro, R. P. S. M. Lobo, N. Bontemps, Z. Konstantinovic, Z. Li, and H. Raffy, *Phys. Rev. Lett.* **88**, 097005 (2002).
- ²⁷ A. F. Santander-Syro, PhD thesis, ESPCI, Paris (2001).
- ²⁸ E. E. Koch, A. Otto, and K. L. Kliewer, *Chem. Phys.* **3**, 362 (1974).
- ²⁹ A. B. Kuzmenko, E. A. Tishchenko, and A. S. Krechetov, *Opt. Spectrosc.* **84**, 402 (1998).
- ³⁰ D. A. Kleinman and W. G. Spitzer, *Phys. Rev.* **121**, 1324 (1961).
- ³¹ J. W. van der Eb, A. B. Kuzmenko, and D. van der Marel, *Phys. Rev. Lett.* **86**, 3407 (2001).
- ³² W. H. Press, B. P. Flannery, S. A. Teukolsky, and W. T. Vetterling, *Numerical Recipes in Fortran*, Cambridge Univ. Press (1986).
- ³³ A. Dienstfrey and L. Greengard, *Inverse Probl.* **17**, 1307 (2001).
- ³⁴ A. B. Djuricic and E. H. Li, *J. Appl. Phys.* **89**, 273 (2001).
- ³⁵ A. B. Kuzmenko, *Guide to Reffit: software to fit optical spectra* (2004), available online at: <http://optics.unige.ch/alexey/reffit.html>.
- ³⁶ H. S. Somal, B. J. Feenstra, J. Schützmann, Jae Hoon Kim, Z. H. Barber, V. H. M. Duijn, N. T. Hien, A. A. Menovsky, M. Palumbo, and D. van der Marel, *Phys. Rev. Lett.* **76**, 1525 (1996).
- ³⁷ F. P. Mena, D. van der Marel, A. Damascelli, M. Fäth, A. A. Menovsky, and J. A. Mydosh, *Phys. Rev. B* **67**, 241101(R) (2003).
- ³⁸ A. B. Kuzmenko, N. Tombros, H. J. A. Molegraaf, M. Grüninger, D. van der Marel, and S. Uchida, *Phys. Rev. Lett.* **91**, 037004 (2003).
- ³⁹ E. M. Vartiainen, K.-E. Peiponen, and T. Asakura, *Appl. Spectrosc.* **50**, 1283 (1996).
- ⁴⁰ G. W. Milton, D. J. Eyre, and J. V. Mantese, *Phys. Rev. Lett.* **79**, 3062 (1997).
- ⁴¹ R. Hulthen, *J. Opt. Soc. Am.* **72**, 794 (1982).
- ⁴² I. Bozovic, *Phys. Rev. B* **42**, 1969 (1990).
- ⁴³ A. B. Kuzmenko, F. P. Mena, H. J. A. Molegraaf, D. van der Marel, B. Gorshunov, M. Dressel, I. I. Mazin, J. Kortus, O. V. Dolgov, T. Muranaka, and J. Akimitsu, *Solid State Commun.* **121**, 479 (2002).
- ⁴⁴ W. G. Spitzer, R. C. Miller, D. A. Kleinman, and L. E. Howarth, *Phys. Rev.* **126**, 1710 (1962).
- ⁴⁵ H. Kuzmany, *Solid State Spectroscopy, an Introduction*, Springer, Berlin, Heidelberg (1998).
- ⁴⁶ U. Bonse and I. Hartmann-Lotsch, *Nucl. Instrum. Methods Phys. Res. A, Accel. Spectrom. Detect. Assoc. Equip.* **222**, 185 (1984).
- ⁴⁷ S. B. White and D. R. McKenzie, *J. Electron Spectrosc. Relat. Phenom.* **43**, 53 (1987).
- ⁴⁸ P. Kielar, *J. Opt. Soc. Am. B, Opt. Phys.* **11**, 854 (1994).
- ⁴⁹ W. Zwerger, *Solid State Commun.* **45**, 841 (1983).
- ⁵⁰ R. A. Ferrell, *Physica C* **152**, 10 (1988).
- ⁵¹ R. L. van Meirhaeghe, E. C. Dutoit, F. Cardon, and W. P. Gomes, *Electrochim. Acta.* **20**, 995 (1975).
- ⁵² T. S. Al'tshuler, I. A. Garifullin, E. G. Kharakhash'yan, and L. F. Shatrukov, *Sov. Phys.- Solid State*, **14**, 2213 (1973).
- ⁵³ J. Jarosz, *Phys. Status Solidi B* **105**, 155 (1981).
- ⁵⁴ C. G. Kinniburgh and J. B. Pendry, *J. Phys. C, Solid State Phys.* **11**, 2415 (1978).
- ⁵⁵ D. Zellouf, Y. Jayet, N. Saint-Pierre, J. Tatibouet, and J. C. Baboux, *J. Appl. Phys.* **80**, 2728 (1996).
- ⁵⁶ J. Mobley, K. R. Waters, and J. G. Miller, *J. Acoust. Soc. Am.* **114**, 2782 (2003).
- ⁵⁷ E. I. Yakubovich, *Sov. Phys.-JETP* **57**, 2120 (1969).
- ⁵⁸ F. Bassani and S. Scandolo, *Phys. Rev. B* **44**, 8446 (1991).